ACS APPLIED MATERIALS & INTERFACES

Research Article

www.acsami.org

Self-Assembly of Gold Nanoparticles on Poly(allylamine Hydrochloride) Nanofiber: A New Route to Fabricate "Necklace" as Single Electron Devices

Rajinder S. Gill,*[,†,#] Ravi F. Saraf,[†] and Subrata Kundu*[,†,§]

[†]Department of Chemical and Biomolecular Engineering, University of Nebraska-Lincoln, Lincoln, Nebraska 68588-0643, United States

[#]Alloy Surfaces Technology Center, 1515 Garnet Mine Road, Boothwyn, Pennsylvania 19060, United States

[§]Electrochemical Materials Science (ECMS) Division, CSIR-Central Electrochemical Research Institute (CECRI), Karaikudi, Tamil Nadu 630006, India

ABSTRACT: Fabrication of a percolating conductive device exhibiting "*necklace-like morphology*" is being reported utilizing a new route. This device was fabricated by exploiting the electrostatic self-assembly of citrate capped negatively charged Au nanoparticles (NPs) (60 nm diameter) over positively charged poly(allylamine hydrochloride) (PAH) fibrous scaffold and followed by synthesis of small Au NPs (~10 nm) on the PAH surface. These 10 nm Au NPs were selectively synthesized over the PAH fiber surface using the surface catalyzed reduction of Au precursor ($HAuCl_4$), leading to a continuous conducting network. This conducting device demonstrated a room temperature (RT) Coulomb-blockade characteristic, which is indicative of "single electron device". The deposition of Au NPs was directed by the diameter of PAH fibers and UV-irradiation exposure time used during the synthesis process. The average diameter of the fibers was in the ~100−150 nm range, and the polyelectrolyte (PAH) was fabricated using the electrospinning technique. The size of these fibers was controlled by tuning the physical properties of PAH solution. Exposure of UV-irradiation for 25 min was sufficiently enough to deposit Au NPs in close proximity to each other. Longer exposure time (~60 min) resulted in a device which showed linear Ohmic current−voltage ($I-V$) behavior. The present process is reproducible, efficient, and resulted in a structurally stable and robust device.

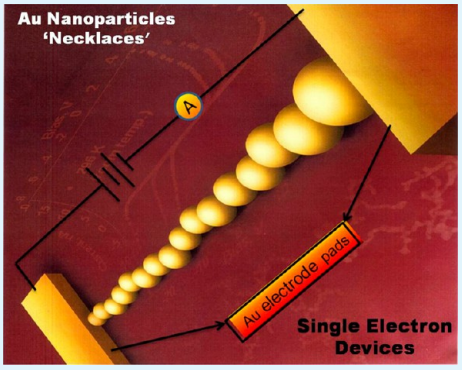

KEYWORDS: *PAH, nanofiber, gold nanoparticles (Au NPs), UV-irradiation, self-assembly, device*

1. INTRODUCTION

During the last couple of years, several nanostructure materials based on nanofibers had been extensively used due to their intriguing chemical and physical properties.[1,2] One dimensional (1-D) nanostructures are good candidates to be used in electronic devices and as sensors. The use of necklace-like morphologies of nanoparticles (NPs) provides a route for the fabrication of single electron devices in which both the surface chemistry and diameter of scaffold can be tailored. Electrospinning techniques have been utilized for the fabrication of a large number of uniform polymers and polyelectrolytes in nanoscale dimensions.[3,4] The electrospinning process is found to be very attractive due to its ability and flexibility to fabricate nanofibers.[5] Electrospinning is a process where a strong electrostatic force is applied to the capillary containing the polymer solution. Initially, fine jets of liquid are formed after applying a sufficient voltage to overcome surface tension and ejected towards a ground target from the tip. At the beginning of the ejection of liquid, a single jet is formed which was subsequently divided into multiple filaments due to radical charge repulsion. The solvent is evaporated during the time of flight and results in the formation of solidified polymer fibers. By regulating the solution physical properties and process parameters, the morphologies of the fibers can be tailored.[6,7]

The dispersion of metal NPs into polymer nanofibers is of great interest due to their novel properties, and there is a continuously growing demand for further miniaturization due to their various types of applications. The incorporation of metal NPs into polymer nanofibers can be achieved by electrospinning polymer solution containing the metal NPs, by self-assembly of metal NPs separately onto the fibrous surface by electrostatic interaction, or by applying surface chemistries on the polyelectrolyte scaffold to synthesize NPs. The electronic properties of metal NPs as a result of single electron transport of current makes them an ideal material for nanodevices. Therefore, metallic or semiconductor NPs decorated over the polymer scaffold generate an exciting system for designing device functionality. Metal NPs with

Received: May 17, 2013
Accepted: September 16, 2013
Published: September 16, 2013

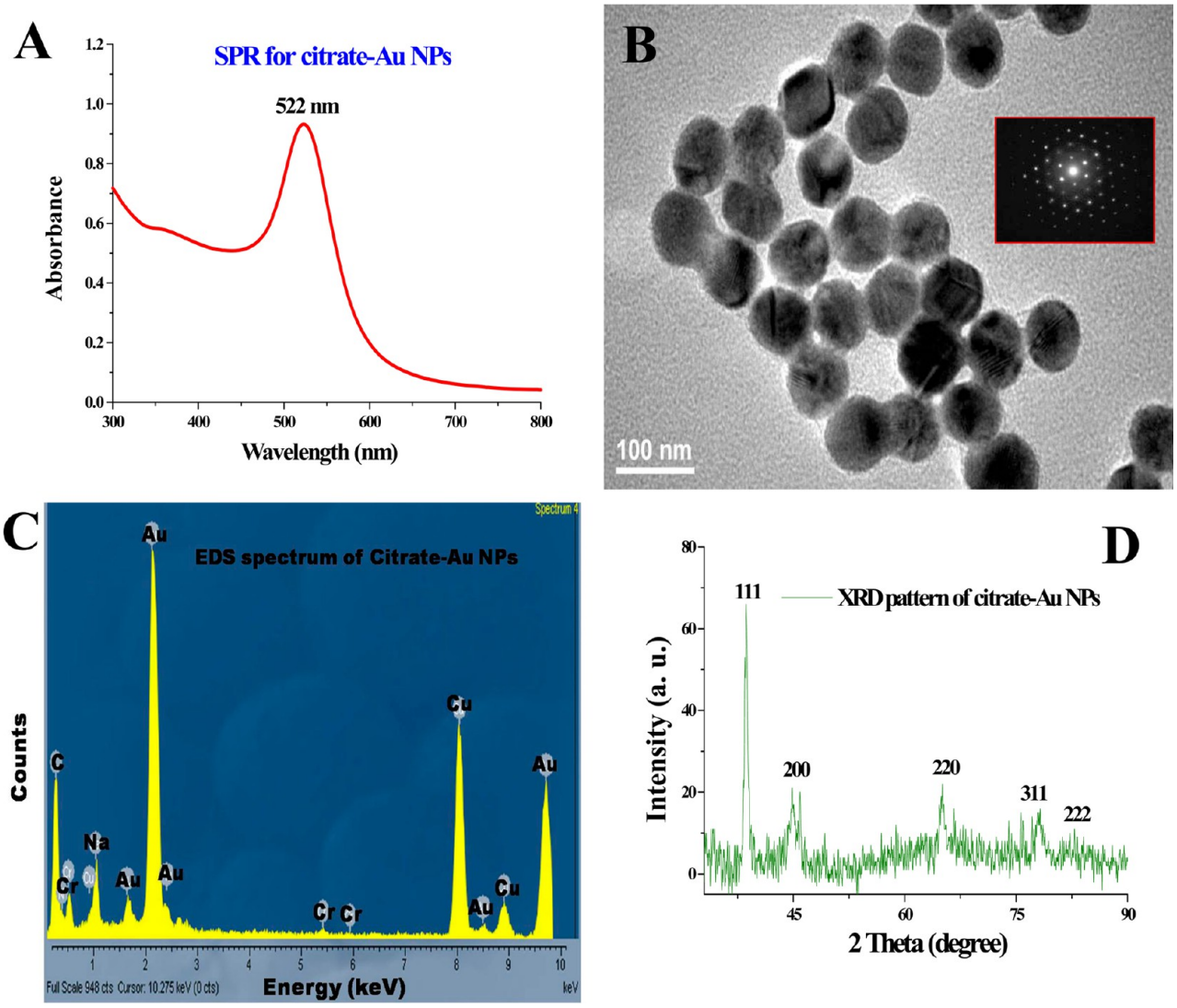

Figure 1. (A) UV−visible spectrum of the citrate coated Au NPs. (B) The transmission electron microscopy (TEM) images of the citrate Au NPs. Inset shows the selected area electron diffraction (SAED) pattern of the same Au NPs. (C) The energy dispersive X-ray spectroscopic (EDS) analysis of the citrate Au NPs. The spectrum shows the expected peaks for Au, Cu, and C. (D) The X-ray diffraction (XRD) pattern of the PAH-Au nanofiber shows the diffraction from the (111), (200), (220), (311), and (222) planes of fcc Au NPs.

electrically percolating clusters show different electrical properties due to their interparticle electron transport.[8] At nano domain, the flow of interparticle current takes place through the transport of a single electron as proved by transport studies on a single-electron,[9] their 2-D and 3-D assemblies,[10,11] and single-electron devices[12] like transistors. Thus, the percolating clusters of metal NPs are shown to be promising candidates to fabricate single-electron devices.

Among the different metal NPs fabricated over fibers, Au NPs are promising because of their unique electronic, optical, and magnetic properties. 1-D arrays of Au NPs within a semicrystalline polymer poly(ethylene) oxide (PEO) were fabricated by Kim and coworkers,[13] and it was observed that there is a 50 nm increase of fiber diameter after addition of Au NPs to PEO. Wang et al. incorporated Au NPs to poly(vinylpyrrolidone) (PVP) by the electrospinning route.[14] Han et al.[15] and Li et al.[16] deposited Au nanostructures over nanofibers utilizing different physical or chemical routes. Dong et al. assembled different metal NPs (Au, Ag, Pt) onto nylon-6 nanofibers by the hydrogen bonding interaction.[17] Sui et al. fabricated self-assembled Au NPs over silica nanofiber by the electrospinning method.[18] There are few other research groups who fabricated polymer nanofibers containing various metal NPs.[19,20] Very recently, few other groups fabricated metal−polymer composite nanofiber by the electrospinning method.[21,22] There are several other reports for the reproducible fabrication of 1-D percolating Au NP assemblies.[23−28] S. Maier's group demonstrated that the 1-D chains of Au NPs can be characterized by studying their spectral position[23] and the inter-particle coupling effect can be utilized for the fabrication of plasmon waveguides in integrated optical devices.[24] Roth's group highlighted the adjustment of size-dependent catalytic, electrical, and optical properties of gold cluster assemblies and discussed significant issues in modern applied nanotechnology.[25] They studied the kinetics of initial nucleation and subsequent cluster growth during sputter deposition of a gold layer over silicon substrate. Recently, Müller-Buschbaum's group studied the growth of Au nanowires over polymers using a novel flow-stream technique.[26] Very recently, the same group demonstrated the structure formation and packing of the

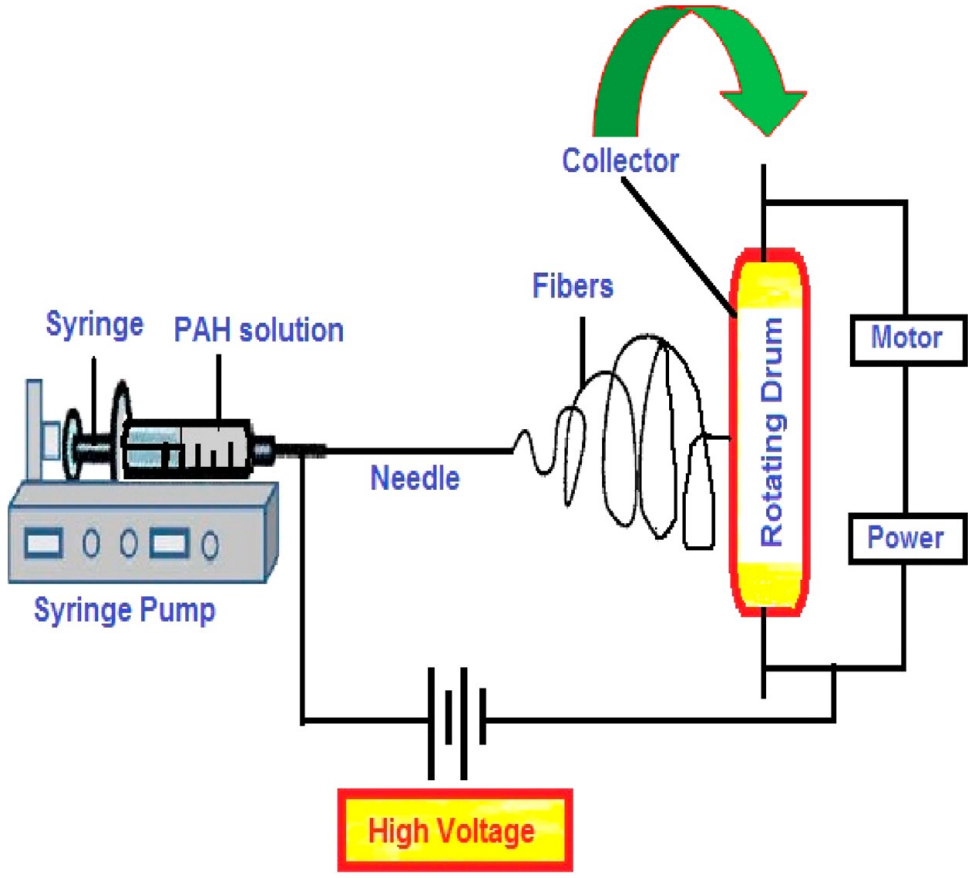

Figure 2. Schematics drawing of the electrospinning setup for the fabrication of PAH nanofibrils.

Au NPs after a 5 s spray cycle deposited over conducting polymer, poly(3-hexylthiophene) (P3HT).[27] Faupel's group reported an easy approach for the fabrication of nanowires using vacuum evaporation techniques.[28]

In the present study, we report a new method for the fabrication of a percolating conductive device exhibiting "*necklace-like morphology*". The fabrication of this device is based on three main process steps. During the first step, polyelectrolyte poly(allylamine hydrochloride), PAH, was fabricated using the electrospinning technique, where we were able to tailor the size of these fibers in the submicrometer size range which was used as a scaffold for NP depositions. Then, the fabricated cationic PAH fibers were decorated with negatively charged, citrate capped Au NPs (60 nm diameter) using electrostatic interactions. During the third step, smaller size Au NPs (~10 nm diameter) were synthesized selectively on the PAH surface using the surface catalyzed reduction of Au precursor ($HAuCl_4$), leading to a continuous conducting network. This device was tested for conductivity measurements and demonstrated a room temperature (RT) Coulomb-blockade characteristic, which is indicative of "single electron devices".

2. EXPERIMENTAL SECTION

2.1. Reagents and Instruments. Hydrogen chloroauric acid ($HAuCl_4{\cdot}3H_2O$), poly(allylamine hydrochloride) (PAH), and dodecyl trimethylammonium bromide (DTAB-99%) were purchased from Sigma-Aldrich and used as received. Citrate capped Au NPs were purchased from BBI International and used as received. De-ionized (DI) water was used for any type of wet chemistry and processing. The Au NPs, the PAH nanofiber, and the deposited Au NPs over PAH nanofiber were characterized using several spectroscopic tools like UV-visible absorption spectra, TEM, EDS, FE-SEM, and XRD analyses. The specification of all these instruments, the process parameters for the electrospinning set-up, UV-irradiation sources, and parameters for conductivity ($I-V$, current−voltage) measurements are given in details in our earlier report.[29]

2.2. Fabrication of PAH Nanofiber by the Electrospinning Method and Selective Deposition of Citrate Coated 60 nm Au NPs over PAH Fiber. The PAH nanofibers were fabricated by the electrospinning method as discussed in detail in our previous work.[29] In brief, an aqueous solution of poly(allylamine) hydrochloride (PAH) (25 wt %) was prepared using DI water. Cationic surfactant, dodecyltrimethylammonium bromide (DTAB), was added to the PAH aqueous solution, which was used to lower the surface tension. Approximately 5−9 wt % of DTAB was optimized to obtain a stable Taylor cone, resulting in nanofibers with uniform size distribution. The importance of the Taylor cone and other specifications for the electrospinning instrument are given elaborately in our earlier paper.[29] The schematics of the electrospinning setup are shown in Figure 2. The substrate containing the PAH nanofibers was immersed in a solution containing citrate capped 60 nm Au NPs overnight, and Au NPs were allowed to self-assemble onto the PAH surface using electrostatic interactions. The tri-sodium citrate capped negatively charged Au NPs were purchased commercially and synthesized using the Turkevich method.[30] The particles were suspended in DI water with a concentration of 1×10^{11} NPs/mL. Then, the chip containing PAH fibers was taken out from the Au NPs suspension, washed with DI water, and dried. The sample was analyzed for Au NPs deposition using FE-SEM analysis. Finally, the chip containing Au NPs deposited on PAH fibers was immersed into $HAuCl_4$ solution which contains 2 mL of 1.23×10^{-4} M $HAuCl_4$ solution and 2 mL of DI water. The chip was exposed to UV-photo-irradiation for 25 min continuously. After UV exposure, the chip was taken out from the solution, rinsed with DI water gently, and then dried. The resultant sample was

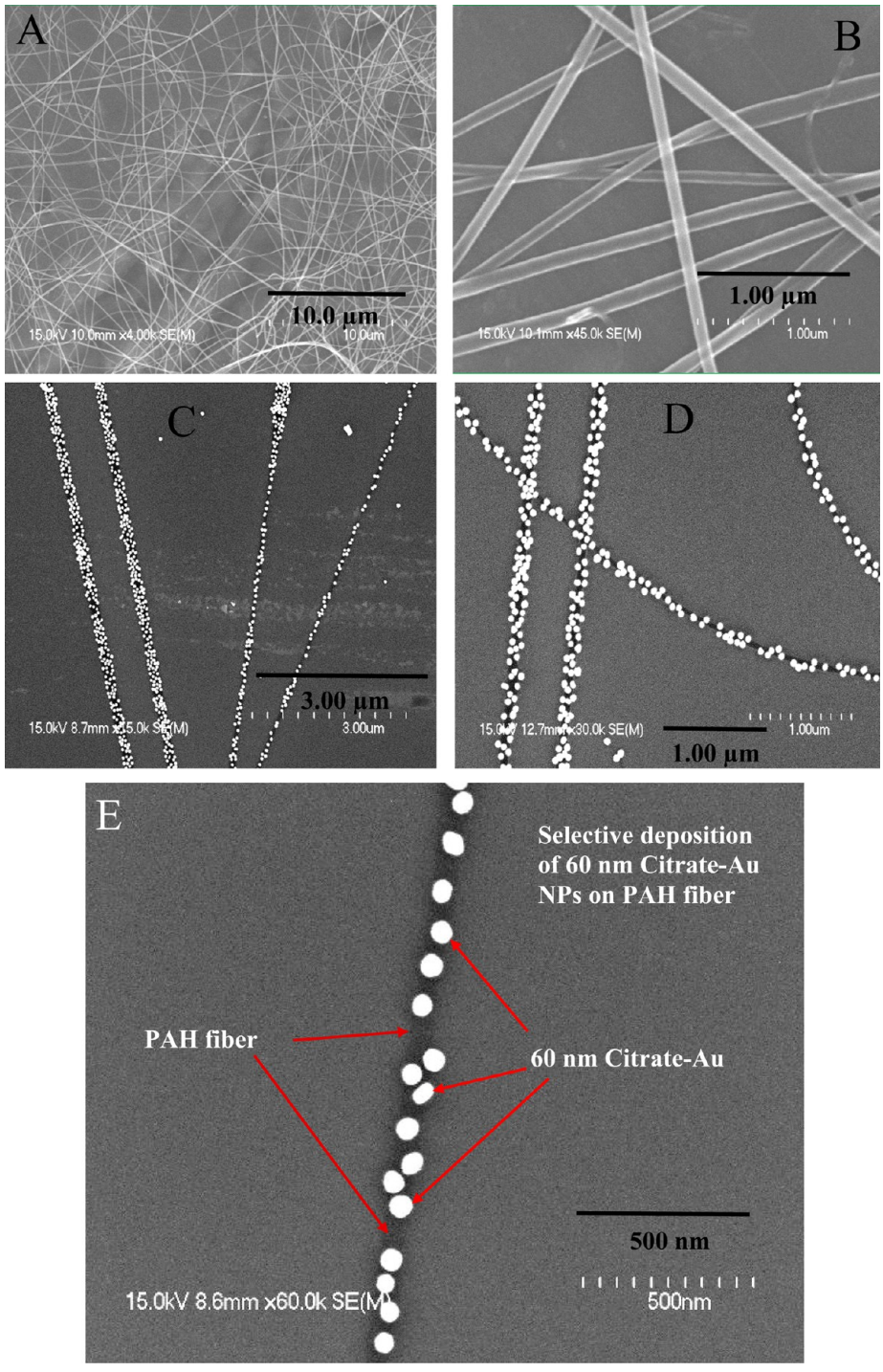

Figure 3. FE-SEM analysis of uncoated PAH fibers (A,B); SEM analysis of 60 nm Au NPs deposited on PAH nanofibrils using electrostatic self-assembly (C–E).

characterized for its surface morphologies using FE-SEM analysis. It was observed that smaller size Au NPs (~10 nm) were synthesized and deposited on a PAH fibrous surface filling the gaps between 60 nm Au NPs. It was observed that 10 nm Au NPs were synthesized selectively on the PAH surface in close proximity to each other and were deposited in between 60 nm Au NPs. Finally, this device was tested for its conductance using two point current–voltage (I–V) measurements.

2.3. Preparation of Samples for Various Characterizations. The negatively charged citrate coated Au NPs were used as received, and the absorbance value was measured using a UV-vis spectrophotometer. The details of sample preparation for the other characterizations like TEM, EDS, XRD, FE-SEM and I–V studies are discussed details in our earlier report.[29]

3. RESULTS AND DISCUSSION

3.1. UV–vis Spectroscopy, Transmission Electron Microscopy (TEM), Energy Dispersive X-ray Spectroscopy (EDS), and X-ray Diffraction (XRD) Analysis. Citrate capped negatively charged Au NPs showed an absorption maxima ~530 nm as shown in the UV–vis spectrum in Figure 1A. The peak at a λ_{max} of 522 nm is due to surface plasmon resonance (SPR) of spherical Au NPs.[31−33] Figure 1B showed

the transmission electron microscopy (TEM) image of the Au NPs at lower magnification. From this analysis, it was found that the average diameter of the Au NPs was ~60 ± 5 nm. The majority of the particles were monodispersed with uniform size distribution. The inset of Figure 1B shows the selected area electron diffraction (SAED) pattern of the Au NPs, which confirmed the single crystalline nature of the Au particles. Figure 1C represents the energy dispersive spectroscopy (EDS) analysis of the Au NPs. The spectra consist of different peaks due to the presence of elements such as C, Cu, and Au. The presence of C and Cu peak is due to the C-coated Cu TEM grid used for TEM analysis, and the Au peak is due to the citrate coated Au NPs solution. Figure 1D shows the X-ray diffraction (XRD) analysis of the citrate coated Au NPs solution which shows diffraction from the (111), (200), (220), (311), and (222) planes of fcc Au NPs with the calculated lattice constant of 0.406 nm matching with the literature (a = 0.4077 nm given by JCPDS file number 4-0784).[34] The XRD pattern of the Au NPs after deposition over PAH fiber was also performed which showed almost similar types of patterns like Figure 1D. On the basis of these characterizations, it was confirmed that the citrate coated Au NPs that were used for our study have a λ_{max} at 530 nm and the average particle size of ~60 ± 5 nm. The detailed studies of the morphology of the fiber after deposition of two different varieties of Au NPs were discussed in detail below using the FE-SEM study.

3.2. Field Emission Scanning Electron Microscopy (FE-SEM) Studies. PAH was fabricated into nonwoven nanofibers using the electrospinning technique. By controlling the solution properties such as concentration, surface tension, and viscosity, a stable Taylor Cone was obtained. A stable Taylor Cone is important to obtain fibers with uniform size distribution. On the basis of EF-SEM analysis, it was found that the diameter of these electrospun fibers ranged from approximately 50 to 150 nm (Figure 3A,B). The average diameter of these fibers was around 100 nm. The diameter of these fibers was controlled by optimizing solution concentration, surfactant to PAH ratios, applied voltage, and the distance between the solution tip and collector. Figure 3C−E represents FE-SEM images under different magnification, where 60 nm Au NPs self-assembled onto PAH fibers using electrostatic interactions. It can be observed that the deposition of Au NPs was directed by the structure of PAH fibers. The self-assembly of Au NPs whether single (singlet), double (doublet), or more was directed by the structural morphology of the polyelectrolyte scaffold. For instance, fibers with an average diameter of approximately 100 nm resulted in a necklace consisting of a 1-D array of 60 nm Au NPs, whereas larger size fibers resulted in clusters of 2 or 3 Au NPs. The interparticle spacing between these particles ranged between 20 and 150 nm. Due to the interparticle repulsion between the negatively charged Au particles, the major challenge was to assemble these particles in close proximity, so that the resultant necklace is conducting. This device was not conducting when the voltage was applied across the electrodes.

In order to make this device percolating, initially, 60 nm citrate capped Au NPs were deposited and finally 10 nm Au NPs were directly synthesized on PAH fibers. The interparticle gaps between 60 nm Au NPs were filled by synthesizing Au NPs using PAH surface catalyzed reduction of $HAuCl_4$ using UV photo-irradiation. The synthesized Au NPs were approximately 10 nm in diameter and were deposited on the PAH surface filling the gaps in between 60 nm Au NPs selectively. The deposition of these particles was fairly discrete,

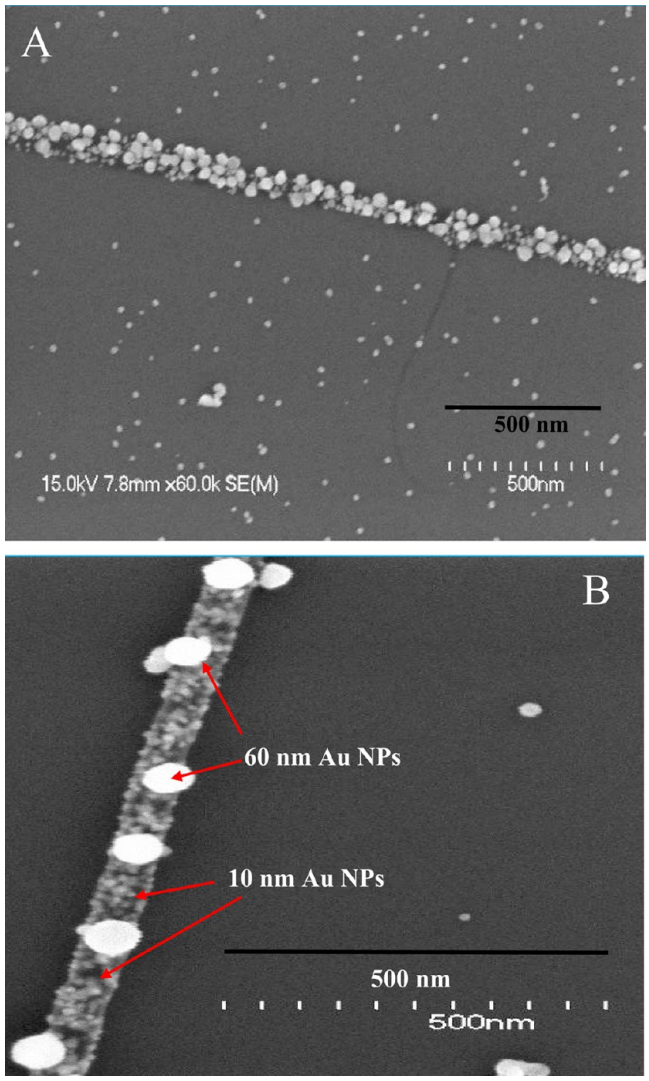

Figure 4. FE-SEM images (A,B) of 60 nm Au NP deposited on PAH fibers followed by controlled deposition of 10 nm Au NP using 25 min of UV-irradiation at different magnifications.

with an interparticle spacing of 1−2 nm. A highly controlled deposition of 10 nm Au NPs was achieved by regulating the UV exposure time. In these nanostructures, there is no special interconnection between the particles beyond the physical contact mediated by the size and morphology of the PAH scaffold. On the basis of FE-SEM analysis (Figure 4A,B), the NPs appears to be percolating due to their close proximity to each other. Figure 4A,B represents the high magnified FE-SEM image of a PAH fiber with Au NPs deposited onto its surface. These images represent the deposition of Au NPs in close proximity to each other, where the deposition of Au NPs was directed by the structure of a scaffold. A longer UV-irradiation exposure time (60 min) resulted in excessive Au NPs deposition leading to a continuous wire-like structure as shown in Figure 5A−C. Similarly, Figure 5A represents a low magnified FE-SEM image showing Au NPs deposition on PAH fibers using 60 min of UV-irradiation exposure time (longer exposure time), connecting two gold pads on the chip. Excessive deposition of Au NPs on the PAH fibrous surface was observed; 60 min of UV-irradiation was used during the 10 nm Au NPs synthesis (see Figure 5B,C).

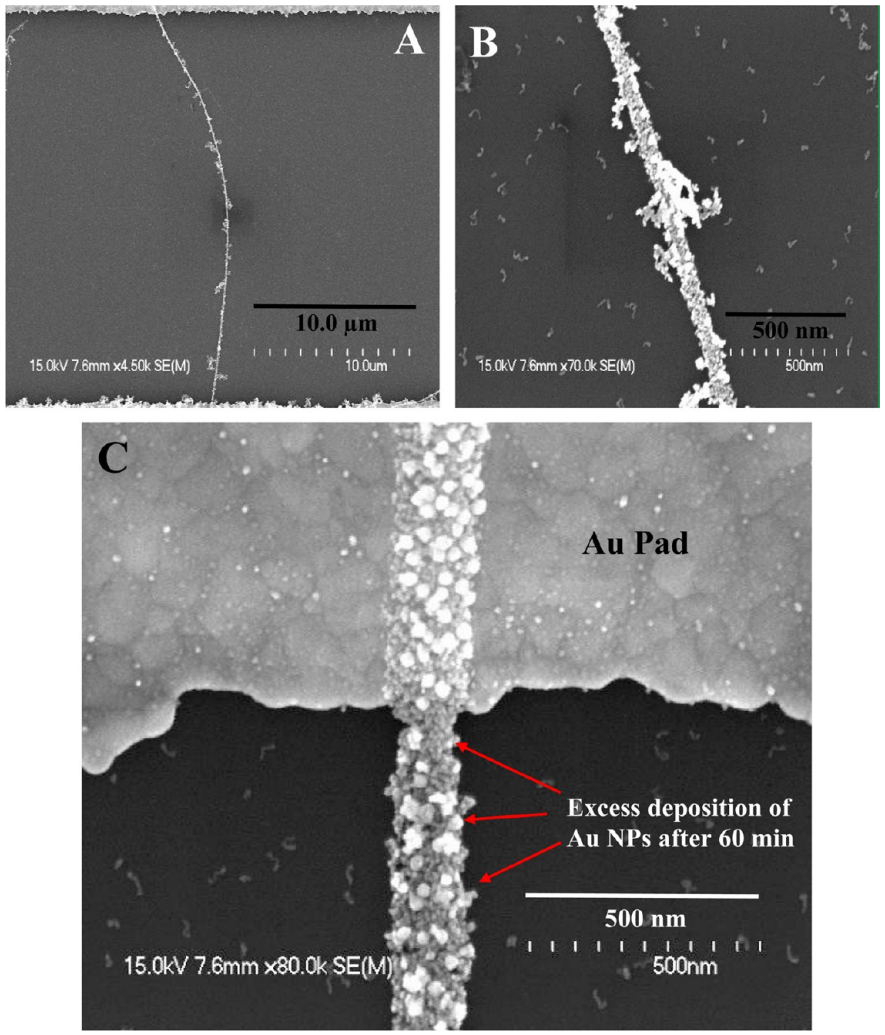

Figure 5. FE-SEM images (A–C) of 60 nm Au NP deposited on PAH fibers followed by excessive deposition of 10 nm Au NP using 60 min of UV-irradiation.

3.3. Mechanism of the Au NPs Deposition over PAH Fiber. Negatively charged citrate capped Au NPs (~60 nm) were deposited onto positively charged PAH nanofibers using electrostatic interactions. The deposition of these NPs was controlled by controlling the diameter of PAH fibers. Thin fibers resulted in 1-D array of NPs, whereas thicker fibers resulted in clusters of NPs deposited on the PAH nanofibers surface. The deposition of these NPs was not in close proximity to make this device as percolating. The average distance between two individual 60 nm Au NPs in close proximity were ~10–20 nm while they were deposited as a single particle in 1-D arrays (as Figure 3E) although in a few places the average distance is little more. Smaller sizes of Au NPs (~10 nm) were synthesized selectively on the PAH surface to make this device percolating. This synthesis was based on the PAH surface catalyzed reduction of $HAuCl_4$ into zero-valent Au NPs in the presence of UV-irradiation. The presence of PAH and controlled UV-photo-irradiation was necessary to synthesize controlled deposition of Au NPs. In the syntheses process, the amino group ($-NH_2$) of PAH acts as reducing agent to reduce $AuCl_4^-$ to Au (0) and oxidize itself to imine.[35] Initially, PAH formed a complex with $AuCl_4^-$, and then, the electron transfer process from polymer to gold ions is initiated in the presence of UV-irradiation. Finally, all the Au^{+3} was reduced to Au(0).[36] The smaller Au NPs (~10 nm) were synthesized and selectively deposited on the PAH fibers, filling the gaps between 60 nm Au NPs. The amount of Au NPs deposited onto PAH fibers was controlled by controlling the UV-irradiation exposure time precisely. Shorter exposure time resulted in discrete Au NPs on PAH fibers, whereas longer exposure time (more than 30 min) resulted in continuous wire type structures as shown in Figure 5C. We believe that larger Au NPs (60 nm) will impart robustness in this device by minimizing the thermal fluctuation effects as compared to smaller Au NPs (10 nm) and those 10 nm Au NPs were synthesized to make this device percolating.

3.4. Conductivity (*I*–*V*) Measurements of This Device. A percolating conductive device exhibiting "*necklace-like morphology*" was used to connect any two Au electrode pads on the chip, which were separated by specified gaps. The conductivity (current–voltage, *I*–*V*) behavior of this device was tested by using a two point probe measurement across Au electrode pads. Figure 6A represents the low magnified FE-SEM image showing a PAH fiber with Au NPs deposited onto its surface, connecting two gold pads on the chip for two point conductivity measurements. It was found that the majority of these Au electrode gaps on the chip, which were connected by PAH/Au NP fibers, were conductive. Figure 6B represents the

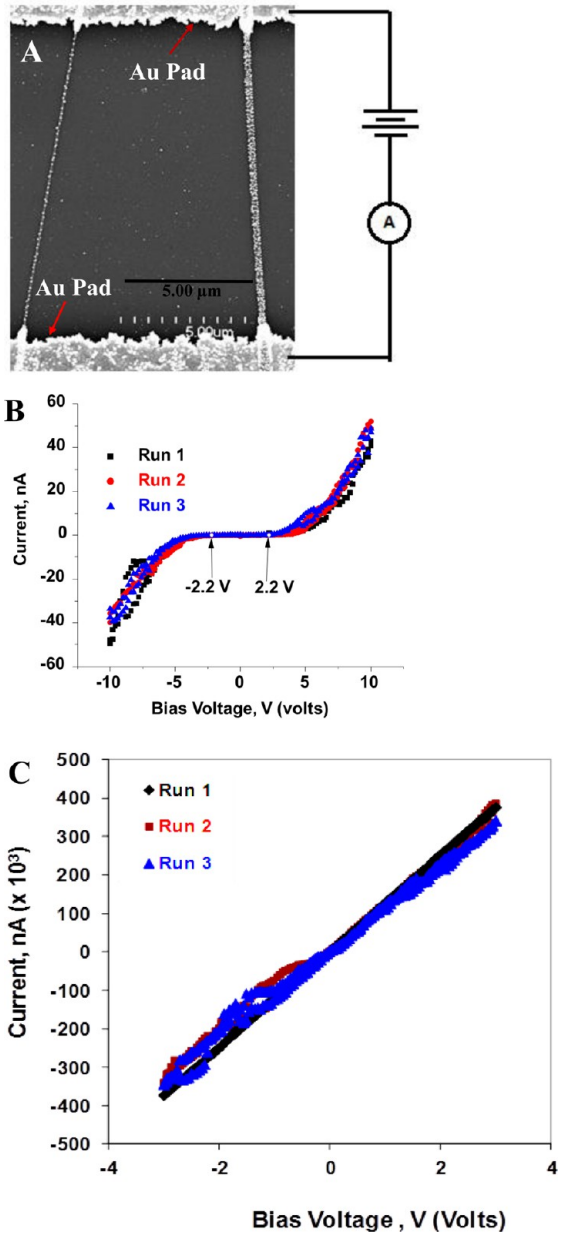

Figure 6. (A) FE-SEM image of the Au NPs deposited over the PAH fiber used for the two points testing in the conductivity measurement. (B) Conductivity (I–V) testing of the device obtained by using 25 min of UV irradiation during Au nanoparticle synthesis. (C) Conductivity (I–V) measurements of the device obtained by using 60 min of UV irradiation during Au NP synthesis.

conductivity measurement across two Au electrode pads separated by a 50 μm gap (largest gap on the chip) connected by Au particles deposited on the PAH fibrous surface. The measurements were made for a bias voltage of −10 to 10 V. This device was conducting with nonlinear current–voltage (I–V) characteristics and a significant threshold bias of V_T is required for current flow. This threshold voltage of 2.2 V was indicative of a Coulomb blockade effect at 298 K as shown in Figure 6B. This observation is consistent with 1-D electron transport that is expected from *necklace-like* morphology device.[37] In single electronics, the charging energy of these particles is inversely proportional to the particle diameter. For smaller sized NPs (conducting islands) with diameter of 10 nm or less, the charging

Scheme 1. Formation of Au NPs "Necklaces" on PAH Fibers

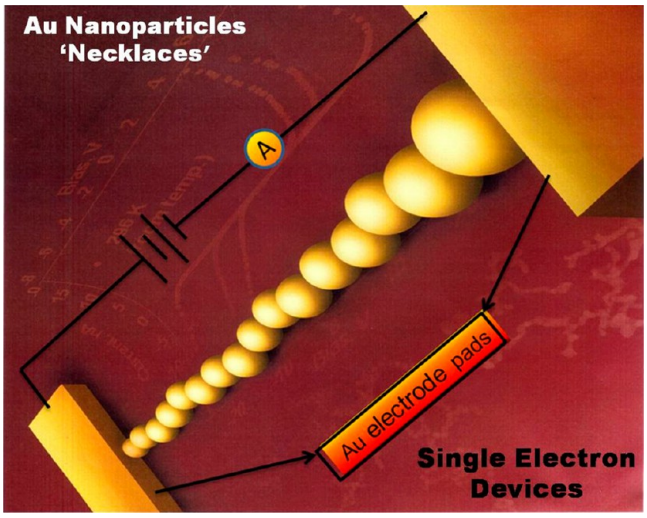

energy of these particles dominates the thermal fluctuations. Consequently, single electron effects can be visible at room temperature.[38] For a device with single isolated particle of diameter d, to be 10 nm, the estimated bias $V_T = e/2C = e/(4\pi\varepsilon\varepsilon_0 d)$ is ∼50 mV corresponding to a barrier energy of 50 meV (2kT at RT), where C is the capacitance, ε_0 is the electric permittivity in vacuum, and ε is the charge of an electron.[39] In our device, discrete 10 nm Au NPs contributed towards the Coulomb blockade effect at RT, whereas larger particles act as conducting wires. These isolated particles are in series, and the net capacitance C_T is given by:

$$\frac{1}{C_T} = \frac{1}{C} + \frac{1}{C} + \frac{1}{C} + \ldots = \frac{n}{C} = \frac{n}{2\pi\varepsilon\varepsilon_0 d}$$

where n is the number of clusters of small NPs. The effective size of the particle is d/n, and coulomb blockade voltage $V_T = e/2C_T = n(e/2C) = nV_1$ (V_1 is the coulomb blockade for a single particle). An increase in the threshold voltage (V_T) from 50 mV for a single particle to 2.2 V for the necklace at RT will require approximately 44 NPs. On the basis of our study, it was found that the resistance of this device was around 2.48×10^8 Ω, which is consistent with the resistance range reported by Loubat et al.[40] for different size range devices. This device was stable and robust during the current–voltage measurements within the limits of bias used. On the other extreme, when the UV exposure time was more than 30 min, it resulted in excessive depositions of 10 nm Au NPs (as shown in Figure 5A–C), making the device behave as a conducting wire. This device exhibits linear Ohmic current–voltage characteristics as shown in Figure 6C. The resistance of this device showing Ohmic behavior was found to be around 4.0×10^3 Ω, which is consistent with that reported by Colm Durkan[41] and Konstantin Likharev[38] for similar type devices. The deposition of Au NPs was controlled by the size of PAH fibers, resulting in a device with "*necklace-like*" morphologies, which was used to control 1-D electronic transport across two Au electrodes as shown in Scheme 1.

4. CONCLUSION

In summary, we were able to fabricate a Au/PAH conductive device which is structurally stable and robust. The deposition of Au NPs was directed by utilizing the structural morphologies of the scaffold and controlling the surface catalyzed syntheses of

dx.doi.org/10.1021/am401864j | ACS Appl. Mater. Interfaces 2013, 5, 9949–9956

Au NPs selectively on the polyelectrolyte (PAH) surface. The resultant device was found to be conductive with nonlinear current−voltage behavior. A significant threshold voltage of 2.2 V was required for current flow, and this threshold voltage is an indication of the Coulomb blockade effect at 298 K and is expected from necklace morphologies. By controlling the polyelectrolyte solution properties, we were able to fabricate fibers having an average diameter in the range of 100 ± 50 nm. The composite nanofiber was nonconducting after the first 60 nm Au NP deposition. During the second stage of depositions, Au NPs were selectively synthesized on the PAH surface using a surface catalyzed reduction of $HAuCl_4$ and UV-irradiation treatment. The average diameter of the synthesized Au NPs was approximately 10 nm. The deposition of 10 nm Au NPs was precisely controlled by regulating the UV-irradiation time and was approximately 25−30 min. Approximately 25 min of UV exposure time was sufficient to make this device percolating. Longer UV-irradiation time showed excessive deposition of Au NPs, and the resultant device was conducting and showed linear Ohmic current−voltage behavior. The diameter of the polyelectrolyte fibers and the deposition of Au NPs were regulated by the process parameters. The present process is extremely efficient, reproducible, and robust. This will provide a route to fabricate structures with *necklace-like* morphologies exhibiting 1-D electron transport. Moreover, we believed that this new polymer−NP memory device could have an important impact in the future of information technology by providing the high-speed, high density memory needed for future advanced computers, digital electronics, and single electron transistors.

AUTHOR INFORMATION

Corresponding Authors

*E-mail: rajinderg@alloysurfaces.com. Phone: (+1) (610) 558-7127. Fax: (+1) (610) 361-7965.
*E-mail: skundu@cecri.res.in. Phone: (+ 91) 4565-241487. Fax: 04565-227651.

Notes

The authors declare no competing financial interest.

ACKNOWLEDGMENTS

National Science Foundation (NSF) with the sanction number NER-0608877 is greatly appreciated for partial funding for this research. S.K. also wishes to acknowledge CSIR-CECRI, Karaikudi for start-up research funding (Project number OLP-0067) for perusing a short part of this work and for preparation of the manuscript.

REFERENCES

(1) Wang, J. F.; Gudiksen, M. S.; Duan, X.; Cui, Y.; Lieber, C. M. *Science* **2001**, *293*, 1455−1457.
(2) Holmes, J. D.; Johnston, K. P.; Doty, R. C.; Korgel, B. A. *Science* **2000**, *287*, 1471−1473.
(3) Huang, Z. M.; Zhang, Y. Z.; Kotaki, M.; Ramakrishna, S. *Compos. Sci. Technol.* **2003**, *63*, 2223−2253.
(4) Li, D.; Xia, Y. *Adv. Mater.* **2004**, *16*, 1151−1170.
(5) Fong, H.; Liu, W.; Wang, C.S.; Vaia, R. A. *Polymer* **2002**, *43*, 775−780.
(6) Ding, Q.; Miao, Y.-E.; Liu, T. *ACS Appl. Mater. Interfaces* **2013**, *5*, 5617−5622.
(7) Jayaraman, K.; Kotaki, M.; Zhang, Y.; Mo, X.; Ramakrishna, S. *J. Nanosci. Nanotechnol.* **2004**, *4*, 52−65.
(8) Su, B.; Goldman, V. J.; Cunningham, J. E. *Science* **1992**, *255*, 313−315.
(9) Crommie, M. F.; Lutz, C. P.; Eigler, D. M. *Science* **1993**, *262*, 218−220.
(10) Andres, R. P.; Bielefeld, J. D.; Henderson, J. I.; Janes, D. B.; Kolagunta, V. R.; Kubiak, C. P.; Mahoney, W. J.; Osifchin, R. G. *Science* **1996**, *273*, 1690−1693.
(11) Middleton, A. A.; Wingreen, N. S. *Phys. Rev. Lett.* **1993**, *71*, 3198−3201.
(12) Sato, T.; Ahmed, H.; Brown, D.; Johnson, B. F. G. *J. Appl. Phys.* **1997**, *82*, 696−701.
(13) Kim, G.; Wutzler, A.; Radusch, H.; Michler, G. H.; Simon, P.; Sperling, R. A.; Parak, W. J. *Chem. Mater.* **2005**, *17*, 4949−4957.
(14) Wang, Y.; Li, Y.; Sun, G.; Zhang, G.; Liu, H.; Du, J.; Yang, S.; Bai, J.; Yang, Q. *J. Appl. Polym. Sci.* **2007**, *105*, 3618−3622.
(15) Han, G. Y.; Guo, B.; Zhang, L. W.; Yang, B. S. *Adv. Mater.* **2006**, *18*, 1709−1712.
(16) Li, D.; McCann, J. T.; Gratt, M.; Xia, Y. N. *Chem. Phys. Lett.* **2004**, *394*, 387−391.
(17) Dong, H.; Wang, D.; Sun, G.; Hinestroza, J. P. *Chem. Mater.* **2008**, *20*, 6627−6632.
(18) Shi, W.; Lu, W.; Jiang, L. *J. Colloid Interface Sci.* **2009**, *340*, 291−297.
(19) Tseng, R. J.; Huang, J.; Ouyang, J.; Kaner, R. B.; Yang, Y. *Nano Lett.* **2005**, *5*, 1077−1080.
(20) Wang, Y.; Yang, Q.; Shan, G.; Wang, C.; Du, J.; Wang, S.; Li, Y.; Chen, X.; Jing, X.; Wei, Y. *Mater. Lett.* **2005**, *59*, 3046−3049.
(21) Lee, C. H.; Tian, L.; Abbas, A.; Kattumenu, R.; Singamaneni, R. *Nanotechnology* **2011**, *22*, 275311−275318.
(22) Jacobs, V.; Anandjiwala, R. D.; Maaza, M. *J. Appl. Polym. Sci.* **2010**, *115*, 3130−3136.
(23) Maier, S. A.; Kik, P. G.; Atwater, H. A. *Appl. Phys. Lett.* **2002**, *81*, 1714−1716.
(24) Maier, S. A.; Kik, P. G.; Atwater, H. A.; Meltzer, S.; Harel, E.; Koel, B. E.; Requicha, A. A. G. *Nat. Mater.* **2003**, *2*, 229−232.
(25) Schwartzkopf, M.; Buffet, A.; Ǩorstgens, V.; Metwalli, E.; Schlage, K.; Benecke, G.; Perlich, J.; Rawolle, M.; Rothkirch, A.; Heidmann, B.; Herzog, G.; Müller-Buschbaum, P.; Ǩohlsberger, R.; Gehrke, R.; Stribeckb, N.; Roth, S. V. *Nanoscale* **2013**, *5*, 5053−5062.
(26) Metwalli, E.; Moulin, J.-F.; Perlich, J.; Wang, W.; Diethert, A.; Roth, S.V.; Müller-Buschbaum, P. *Langmuir* **2009**, *25*, 11815−11821.
(27) Al-Hussein, M.; Schindler, M.; Ruderer, M. A.; Perlich, J.; Schwartzkopf, M.; Herzog, G.; Heidmann, B.; Buffet, A.; Roth, S. V.; Müller-Buschbaum, P. *Langmuir* **2013**, *29*, 2490−2497.
(28) Adelung, R.; Aktas, O. C.; Franc, J.; Biswas, A.; Kung, R.; Elbahri, M.; Kanzov, J.; Schurmann, U.; Faupel, F. *Nat. Mater.* **2004**, *3*, 375−379.
(29) Kundu, S.; Gill, R. S.; Saraf, R. F. *J. Phys. Chem. C* **2011**, *115*, 15845−15852.
(30) Turkevich, J.; Stevenson, P. C.; Hillier, J. *Discuss. Faraday Soc.* **1951**, *11*, 55−75.
(31) Kundu, S.; Maheshwari, V.; Saraf, R. F. *Langmuir* **2008**, *24*, 551−555.
(32) Kundu, S.; Peng, L.; Liang, H. *Inorg. Chem.* **2008**, *47*, 6344−6352.
(33) Kundu, S.; Lau, S.; Liang, H. *J. Phys. Chem. C* **2009**, *113*, 5150−5156.
(34) Guinier, A. *X-Ray Diffraction*; W. H. Freeman and Company: San Franscisco, CA, 1963.
(35) Keene, F. R. *Coord. Chem. Rev.* **1999**, *187*, 121−149.
(36) Kuo, P. L.; Chen, C. C.; Jao, M. W. *J. Phys. Chem. B* **2005**, *109*, 9445−9450.
(37) Lopes, W. A.; Jaeger, H. M. *Nature* **2001**, *414*, 735−738.
(38) Likharev, K. K. *Proc. IEEE* **1999**, *87*, 606−632.
(39) Maheshwari, V.; Kane, J.; Saraf, R. F. *Adv. Mater.* **2008**, *20*, 284−287.
(40) Loubat, A.; Escoffier, W.; Lacroix, L.-M.; Viau, G.; Tan, R.; Carrey, J.; Warot-Fonrose, B.; Raquet, B. *Nano Res.* **2013**, *6*, 644−651.
(41) Durkan, C. *Current at the Nanoscale: An Introduction to Nanoelectronics*; Imperial College Press: London, 2007.